Modeling drifting snow in Antarctica with a regional climate model: 1. Methods and model evaluation

J. T. M. Lenaerts,[1] M. R. van den Broeke,[1] S. J. Déry,[2] E. van Meijgaard,[3] W. J. van de Berg,[1] Stephen P. Palm,[4] and J. Sanz Rodrigo[5]

Received 22 April 2011; revised 19 December 2011; accepted 30 December 2011; published 6 March 2012.

[1] To simulate the impact of drifting snow on the lower atmosphere, surface characteristics and surface mass balance (SMB) of the Antarctic ice sheet regional atmospheric climate model (RACMO2.1/ANT) with horizontal resolution of 27 km is coupled to a drifting snow routine and forced by ERA-Interim fields at its lateral boundaries (1989–2009). This paper evaluates the near-surface and drifting snow climate of RACMO2.1/ANT. Modeled near-surface wind speed (squared correlation coefficient $R^2 = 0.64$) and temperature ($R^2 = 0.93$) agree well with observations. Wind speed is underestimated in topographically complex areas, where observed wind speeds are locally very high (>20 m s^{-1}). Temperature is underestimated in winter in coastal areas due to an underestimation of downward longwave radiation. Near-surface temperature and wind speed are not significantly affected by the inclusion of drifting snow in the model. In contrast, relative humidity with respect to ice increases in regions with strong drifting snow and becomes more consistent with the observations. Drifting snow frequency is the only observable parameter to directly validate drifting snow results; therefore, we derived an empirical relation for fresh snow density, as a function of wind speed and temperature, which determines the threshold wind speed for drifting snow. Modeled drifting snow frequencies agree well with in situ measurements and novel estimates from remote sensing. Finally, we show that including drifting snow is essential to obtaining a realistic extent and spatial distribution of ablation (SMB < 0) areas.

Citation: Lenaerts, J. T. M., M. R. van den Broeke, S. J. Déry, E. van Meijgaard, W. J. van de Berg, S. P. Palm, and J. Sanz Rodrigo (2012), Modeling drifting snow in Antarctica with a regional climate model: 1. Methods and model evaluation, *J. Geophys. Res.*, *117*, D05108, doi:10.1029/2011JD016145.

1. Introduction

[2] The surface mass balance (SMB), together with the solid ice discharge across the grounding line (D), determines the mass balance (MB) of the Antarctic ice sheet (AIS):

$$MB = SMB - D \tag{1}$$

[3] Recent estimates suggest that MB < 0, i.e., D exceeds SMB and the AIS is losing mass and contributes to sea level rise (SLR) [*Rignot et al.*, 2008; *Velicogna*, 2009] at rates of about 100–200 Gt yr^{-1} (~0.3–0.6 mm yr^{-1} SLR). These estimates are uncertain, in part because of large remaining uncertainties in SMB. The specific SMB (SSMB) of a snow/ice surface (kg m^{-2} yr^{-1}) can be written as the annual sum of precipitation (P), surface sublimation (SU_s), runoff due to melt (RU) and erosion by (ER_{ds}) and sublimation of drifting snow (SU_{ds}) per unit area:

$$SSMB = \int_{year} (P - SU_s - RU - ER_{ds} - SU_{ds})dt \tag{2}$$

where ER_{ds} equals the divergence of the horizontal transport of snow (TR_{ds}). Note that we define drifting snow here as the combined processes of drifting snow particles, which are limited to below 2 m above the surface, and blowing snow particles (above that level). Until now, drifting snow erosion and sublimation have been neglected in the majority of Antarctic SMB studies [*Turner et al.*, 1999; *Genthon and Krinner*, 2001; *Van de Berg et al.*, 2005, 2006]. Various efforts to quantify the effects of drifting snow suggest that drifting snow sublimation may be of importance on a continent-wide scale, not only in Antarctica [*Budd*, 1966; *Bintanja*, 1998; *Déry and Yau*, 2001; *Van den Broeke et al.*, 2006], but also in other snow covered regions, such as the

[1]Institute for Marine and Atmospheric Research Utrecht, Utrecht University, Utrecht, Netherlands.
[2]Northern Hydrometeorology Group, University of Northern British Columbia, Prince George, Canada.
[3]Royal Netherlands Meteorological Institute, De Bilt, Netherlands.
[4]Science Systems and Applications, Inc., NASA Goddard Space Flight Center, Greenbelt, Maryland, USA.
[5]Von Karman Institute for Fluid Dynamics, Rhode-St.-Genese, Belgium.

0148-0227/12/2011JD016145

Greenland ice sheet [*Box et al.*, 2006] and the Canadian plains in winter and spring [*Pomeroy and Essery*, 1999].

[4] A major research obstacle is that modeling of drifting snow requires a high horizontal and vertical resolution; for instance, topographic features that determine the direction and speed of the katabatic wind in Antarctica and enhance accumulation on the upwind side [*Van den Broeke et al.*, 1999; *Frezzotti et al.*, 2005] must be well resolved.

[5] All SMB components including snow transport and drifting snow sublimation are strongly controlled by the overlying atmosphere. Due to its remote location and harsh weather conditions, drifting snow measurements on the AIS are sparse in time and space [*Bintanja*, 2000; *Mann et al.*, 2000; *Mahesh et al.*, 2003; *Van As et al.*, 2007]. That is why drifting snow data from measurement campaigns performed during the International Geophysical Year (IGY, 1957–1958) are still useful today. For example, *Loewe* [1970] compiled wind speeds and drifting snow frequencies at 18 ice sheet stations under highly different atmospheric and surface conditions, providing excellent insight in the spatial variability of drifting snow on the AIS.

[6] To support the interpretation of in situ observations, regional climate models have provided continent-wide information on the climate and SMB of the large ice sheets of Antarctica [*Van de Berg et al.*, 2005; *Bromwich et al.*, 2004] and Greenland [*Fettweis*, 2007; *Box et al.*, 2006; *Ettema et al.*, 2009]. Conversely, for these models to be credible, evaluation of the near-surface climate using in situ observations is essential [*Ettema et al.*, 2010a].

[7] Here we describe the implementation of a drifting snow routine in the regional atmospheric climate model RACMO2.1/ANT, which has been especially adapted to simulate polar climate conditions [*Van de Berg et al.*, 2005]. Part 2 of this paper [*Lenaerts and van den Broeke*, 2012] describes the results, i.e., the drifting snow climate of the AIS and how it interacts with the SMB and the lower atmosphere. Part 1 (the present paper) describes the methodology and evaluation of RACMO2.1/ANT over the AIS, and is structured as follows: In section 2, we present the methods. Section 3 describes the evaluation of the near-surface conditions and drifting snow frequency, and section 4 finishes with conclusions.

2. Methods

2.1. Drifting Snow Scheme

[8] To calculate TR_{ds}, simple relations have been proposed between friction velocity (u_*) and drifting snow flux [e.g., *Mann et al.*, 2000]. The parameterizations for SU_{ds} are computationally much more expensive, mainly because of the multiple snow particle size classes involved [*Xiao et al.*, 2000]. As an alternative, *Déry and Yau* [1999] proposed a bulk (i.e. non-spectral) parameterization for both components of the drifting snow process; based on single-level input of temperature, specific humidity, pressure and wind speed, this parameterization calculates a vertical profile of the thermodynamic variables as well as a new 'bulk' variable (q_b), which determines the ratio of mass of suspended snow particles to that of air [*Déry and Yau*, 1999].

[9] The column-integrated rates of sublimation (m s^{-1}) and transport (kg m^{-1} s^{-1}) are defined as:

$$SU_{ds} = \int_{z_{lb}}^{z_{ub}} S_b dz \tag{3}$$

$$TR_{ds} = \rho \int_{z_{lb}}^{z_{ub}} U q_b dz \tag{4}$$

where S_b is the local sublimation rate [kg kg^{-1} s^{-1}], U is the horizontal wind speed [m s^{-1}], and z_{lb} and zu_{ub} denote the height of the lower and upper boundary of the drifting snow layer [m]. Of particular importance are the assumptions made at these boundaries. At z_{lb}, which is defined to be at the snow surface, the air is assumed to be saturated with respect to ice. The specific humidity profile decreases with height above the surface following a logarithmic function, while temperature is assumed to be constant with height. This implies a strongly decreasing relative humidity (RH) with height. In the drifting snow layer, zero fluxes of heat, moisture or snow particles are imposed at the upper boundary. A more detailed description of the drifting snow routine is given by *Déry and Yau* [1999].

[10] Several changes were made to the original drifting snow model of *Déry and Yau* [1999]. First, we decreased the vertical resolution as well as the number of size classes in the gamma distribution to increase computational speed. The vertical profile now has 12 layers, of which 7 are located in the lowest 20 m of the atmosphere. As most of the drifting snow events are limited to the lowest few meters, the reduced vertical resolution does not significantly affect the column-integrated amount of drifting snow [*Lenaerts et al.*, 2010]. Similarly, the amount of size classes to determine the snow particle spectrum is reduced from 64 to 32. Winds are relatively strong on the Antarctic ice sheet, while temperatures are low; this favors the breaking and rounding of snow crystals. This means that the drifting snow crystals are generally small [*Gallée et al.*, 2001] so the size spectrum is narrow.

[11] Secondly, instead of assuming a temperature that is constant with height, we applied a more realistic dry-adiabatic temperature lapse rate to the profile, such that SU_{ds} is reduced in higher layers due to lower temperatures. Whereas the lower troposphere in Antarctica is usually characterized by a strong temperature inversion in calm conditions, strong winds to a large extent enhance turbulent mixing. With these changes, a sensitivity test with the single column model version of RACMO2.1/ANT led to a drifting snow sublimation change of less than 5% at Neumayer base, East Antarctica [*Lenaerts et al.*, 2010].

[12] *Yang and Yau* [2008] show that drifting snow characteristics produced by PIEKTUK compare well with observations from, among others, two Antarctic stations. Despite its relative simplicity, various comparison studies show that this bulk parameterization yields results that are very similar to computationally more expensive spectral drifting snow models [*Déry and Yau*, 1999; *Xiao et al.*, 2000].

2.2. Regional Climate Model Description

[13] We used the Regional Atmospheric Climate Model version 2.1 to simulate present-day Antarctic climate

conditions (RACMO2.1/ANT hereafter). The atmospheric dynamics in RACMO2.1/ANT are from the High Resolution Limited Area Model (HIRLAM, version 5.0.6. [*Undén et al.*, 2002]), while the description of the physical processes is adopted from the European Centre for Medium-Range Weather Forecasts (ECMWF, cycle 23r4 [*White*, 2001]). The model domain includes the Antarctic continent and a part of the surrounding Southern Ocean (Figure 1). The quasi-rectangular grid measures 240 by 262 points, resulting in a horizontal resolution of around 27 km. Figures 1b and 1c compare the resolution of RACMO2.1/ANT with ERA-Interim (∼80 km horizontal resolution). Individual glacial valleys are much better resolved at 27 km, which may be critical for the simulation of drifting snow transport.

[14] At its lateral boundaries, RACMO2.1/ANT is forced by the ECMWF four-dimensional variational (4D-Var) reanalysis ERA-Interim (1989 to present [*Simmons et al.*, 2007]). The forcing is prescribed every 6 hours, whereas the model interior is allowed to evolve freely. A previous simulation with RACMO2.1/ANT [*Van de Berg et al.*, 2005, 2006] used ERA-40 (1957–2002) as forcing, supplemented with operational analyses (September 2002 - December 2004). Compared to ERA-40, ERA-Interim has higher horizontal resolution, more data assimilated and updated model physics [*Simmons et al.*, 2007]. As no coupling to an ocean model is present, sea-ice extent, thickness and sea surface temperature are prescribed. RACMO2.1/ANT has 40 vertical hybrid-levels that are terrain-following close to the surface and become pressure levels at higher altitudes. The lowest model level is at approximately 10 m above the surface. RACMO2.1/ANT has proven to realistically simulate the climate and SMB of Antarctica [*Van de Berg et al.*, 2005; *Van de Berg et al.*, 2006; *Lenaerts et al.*, 2012] and Greenland [*Ettema et al.*, 2009].

[15] Adjustments to the original formulation of the dynamical and physical processes in RACMO2.1 are described by *Van Meijgaard et al.* [2008]. Apart from that, several changes were implemented to better simulate ice sheet climate: the roughness length formulation was changed [*Reijmer et al.*, 2005] and the ratio between liquid and solid precipitation at low temperatures decreased [*Van de Berg et al.*, 2006]. For our goal, which is to realistically simulate drifting snow, an accurate representation of the snow surface and sub-surface processes is necessary [*Gallée et al.*, 2001]. The updated snow model in RACMO2.1/ANT considers important physical processes in the snowpack, such as meltwater percolation, retention and refreezing, and correctly treats the interaction between the snow/firn/ice surface and the atmosphere [*Ettema et al.*, 2010a]. For instance, using RACMO2.1 with the updated snow model at ∼11 km resolution over the Greenland ice sheet, *Ettema et al.* [2009] found that 45% of the meltwater in Greenland does not run off, but refreezes in the snowpack. Another recent model improvement concerns snow albedo, which is vital to calculate the energy budget at the surface, and for a large part determines the availability of melt energy [*Van den Broeke et al.*, 2010]. Although the largest portion of the meltwater refreezes locally in Antarctica, melting strongly impacts the surface snow layers: it increases the snow grain size, the water content of the snow and thereby its density [*Kuipers Munneke et al.*, 2011]. As a result, melting strongly reduces the potential for drifting snow [*Lenaerts and van den Broeke*, 2012]. These considerations urged the development of a new albedo scheme, which is described in detail by *Kuipers Munneke et al.* [2011].

[16] Firn densification in RACMO2.1/ANT is modeled according to *Pimienta and Duval* [1987], but in the upper 5–10 m, we use the time-dependent densification expression modified from *Arthern et al.* [2010]. Apart from annual mean temperature and accumulation, this scheme needs a surface density value, i.e. a value for fresh snow. This parameter is also critical for drifting snow onset, and is discussed separately in section 2.4.

2.3. Coupling the Drifting Snow Routine to RACMO2.1/ANT

[17] Drifting snow sublimation (SU_{ds}) and erosion (ER_{ds}) are processes that remove/deposit mass from/on the snow surface. Moreover, SU_{ds} adds moisture to and extracts heat and momentum from the atmospheric surface layer (SL). The state of the snow surface determines how susceptible particles are to be picked up by the wind. Therefore, a direct coupling of the drifting snow routine both with the lower atmosphere and the snow surface scheme in RACMO2.1/ANT is essential.

[18] Drifting snow starts when the friction velocity (u_*) exceeds a certain threshold value $u_{*,t}$. The friction velocity u_* is a function of the surface layer wind speed (here we use 10 m wind speed (U_{10m})) and the surface roughness length z_0, assuming a logarithmic wind profile during strong wind conditions (neutral stability [*Garratt*, 1992]).

[19] The surface roughness length z_0 is determined by the shape of the surface roughness elements and the prevailing wind direction, the combination of which determines the effective area of roughness elements [*Lettau*, 1969]. In Antarctica, a wide range of surface roughness elements is found, from smooth blue ice to rough sastrugi. As a result, a wide range of z_0 values have been reported for Antarctic surfaces; they range from <0.1 mm over blue ice [*Bintanja and van den Broeke*, 1995], 0.1–0.2 mm over Brunt ice shelf [*King and Anderson*, 1994], Fimbul ice shelf [*Liljequist*, 1956], and over snow on the Antarctic interior plateau [*Weller*, 1980], ∼0.3 mm over ice crust at Mizuho Plateau [*Fujii and Kusunoki*, 1982], ∼0.8 mm over low sastrugi in Dronning Maud Land [*Bintanja and van den Broeke*, 1995], ∼1 mm in Adlie Land, Antarctica [*Wendler et al.*, 1988] and >10 mm when the prevailing wind is directed toward the elongated sides of high sastrugi [*Jackson and Carroll*, 1978]. In summary, generally lower values are reported from the inland plateau and coastal ice shelves, where katabatic winds are absent, and higher values from the marginal slopes, where katabatic winds are active. However, insufficient information is available to map z_0 spatially and temporally, so at present there is no justification to prescribe a spatially varying field of z_0, and we decided to use a value of 1 mm over the grounded ice sheet as well as the ice shelves. Using this constant z_0, a realistic near-surface wind field over Antarctica is simulated [*Reijmer et al.*, 2004]. A well-known phenomenon is the apparent increase of z_0, z_h and z_q during blowing snow conditions, [*Bintanja and Reijmer*, 2001]. This is not caused by changes in the surface characteristics, but by the altered wind, temperature and humidity profiles, i.e. it is a result of rather than feeding back

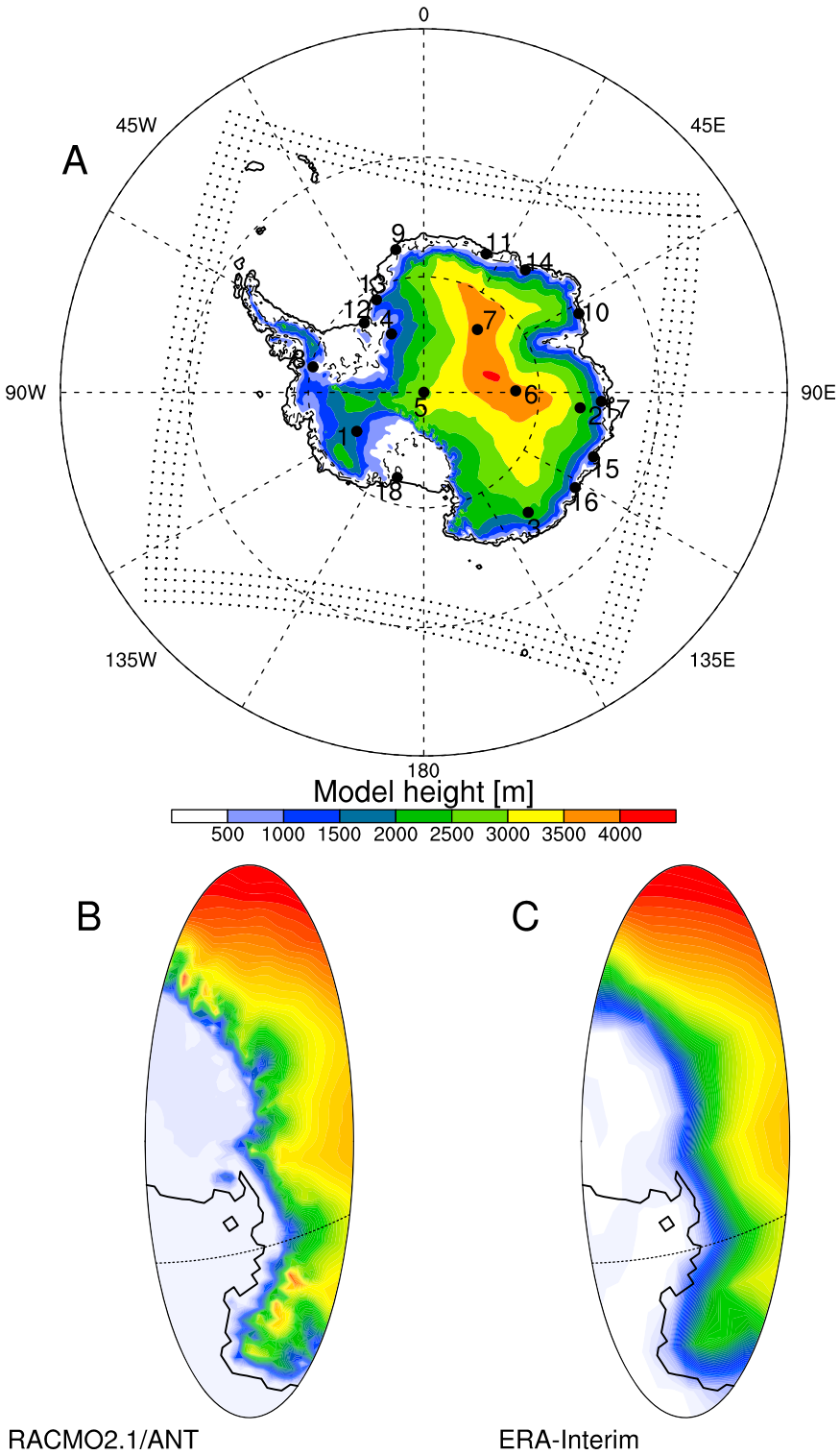

Figure 1. (a) Map of Antarctica, including ice shelves, showing the model domain (outer border of area), relaxation zone (dotted area, 16 grid points) and the model topographic height (colors). (b and c) Comparison of model topography in Victoria Land (70–85°S, 150–180°E) according to RACMO2.1/ANT (~27 km, Figure 1b) and ERA-Interim (about 80 km, Figure 1c). The scale runs from 0 (white) to 3000 m (red) above sea level. The location of the stations used for the fresh snow density parameterization are indicated in Figure 1a.

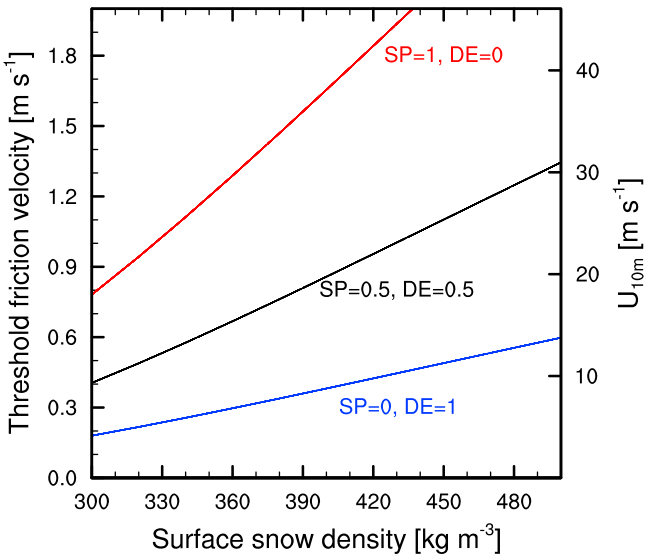

Figure 2. Threshold friction velocity ($u_{*,t}$) and corresponding 10 m wind speed (U_{10m}) for neutral stability as a function of surface snow density (ρ_s) for varying snow mobility characteristics. Roughness length for momentum z_0 is assumed to be constant at 1 mm. After *Gallée et al.* [2001].

on snow particle sublimation. To avoid unrealistic feedbacks, the blowing snow routine does not require input for z_0, z_h and z_q, but rather uses values for wind speed, temperature and humidity at a fixed level above the surface, either from observations [*Lenaerts et al.*, 2010] or (as in our case) from the first model level.

[20] The expression for the threshold friction velocity $u_{*,t}$ is defined as [*Gallée et al.*, 2001]

$$u_{*,t} = u_{*,t_0} \exp\left(\frac{-n}{1-n} + \frac{n_0}{1-n_0}\right) \tag{5}$$

where n is the snow porosity:

$$n = 1 - \frac{\rho_s}{\rho_i} \tag{6}$$

and, similar for n_0:

$$n_0 = 1 - \frac{\rho_0}{\rho_i} \tag{7}$$

in which ρ_s is the actual snow density (the mean of the upper 5 cm of snow) and ρ_i the density of ice (both in [kg m^{-3}]). n_0, similarly, is defined as the porosity of fresh snow (a value of 300 kg m^{-3} for ρ_0 is used here). u_{*,t_0} is defined as [*Gallée et al.*, 2001]

$$u_{*,t_0} = \frac{\log(2.868) - \log(1+Mo)}{0.085} C_D^{0.5} \tag{8}$$

[21] C_D is the drag coefficient for momentum:

$$C_D = \frac{{u_*}^2}{U^2} \tag{9}$$

with U denoting near-surface wind speed [m s^{-1}]. A typical value of C_D is 0.002 for a neutral surface layer, a surface roughness for momentum z_0 of 1 mm and U is measured at 10 m above the surface.

[22] In equation (8), Mo describes the mobility of snow particles [*Gallée et al.*, 2001]:

$$MO = 0.75DE - 0.5SP + 0.5 \tag{10}$$

[23] Dendricity (DE) varies from 0 (old snow) to 1 (fresh snow), depending on the number of fresh snow grain shapes remaining in the snow layer. Sphericity (SP) also varies between 0 (completely angular) and 1 (completely rounded), and represents the ratio of rounded to angular snow grains in the snowpack.

[24] Figure 2 shows that for a sphericity and dendricity of 0.5 (black line) the threshold friction velocity increases nearly linearly from 0.4 m s^{-1} for ρ_s of 300 kg m^{-3} to 1.35 m s^{-1} when ρ_s equals 500 kg m^{-3}. For z_0 = 1 mm, DE = 1 and SP = 0, drifting snow starts ($u_* = u_{*,t}$) even at relatively low 10 m wind speeds (~7 m s^{-1}) when the surface snow density is below 350 kg m^{-3}. When the snow surface is more consolidated (ρ_s > 500 kg m^{-3}) and snow grains are rounded (SP = DE = 0.5), e.g. after melt events, U_{10m} > 30 m s^{-1} is required to activate drifting snow. We conclude that drifting snow onset is very sensitive to surface snow density and grain shape, which determines mobility.

[25] Explicitly modeling the evolution of snow mobility requires detailed prognostic computations of snow particle characteristics, with very limited observational data to evaluate the results for the AIS. Moreover, data are also needed for ρ_s, a poorly defined variable in the field for which similarly few observations are available. However, drifting snow frequency is a more commonly observed variable at Antarctic stations. That is why we choose to adopt constant values for SP (0.5) and DE (0.5), implying a snow mobility index of 0.625, and develop a parameterization for surface snow density, such that modeled drifting snow frequencies agree with observations (see section 2.4). By fixing DE and SP, the result of the iterative procedure is a local surface snow density that is not necessarily realistic, but merely provides a realistic drifting snow frequency for that location.

[26] To achieve the atmospheric coupling, the drifting snow routine is included in the turbulent diffusion scheme of RACMO2.1/ANT, which accounts for momentum, heat and moisture exchange at the surface [*Lenaerts et al.*, 2010]. Temperature (T), specific humidity (q_v), wind speed (U) and pressure (p) at the lowest model level (~10 m) are first fed into the drifting snow routine to calculate SU_{ds} and TR_{ds}. Specific humidity is converted to relative humidity with respect to ice (RH_i) using the expression proposed by *Hyland and Wexler* [1984]. If drifting snow occurs in the model, SU_{ds} is calculated and expressed in units of an energy flux (W m^{-2}). During drifting snow, this is assumed to be the only source of latent heat exchange at the surface, extracting heat from the surface and adding moisture to the surface layer (SL). This is realistic, because the near-surface air readily becomes saturated due to the drifting snow sublimation process itself, prohibiting surface sublimation (SU_s = 0 [*Bintanja*, 2001]). The moisture released by SU_{ds} then automatically mixes into the atmospheric boundary

layer (ABL) through the turbulent diffusion scheme of RACMO2.1/ANT. The formulation of the sensible heat flux remains unaltered.

[27] The chain of events is as follows: during drifting snow, $SU_s = 0$, but $SU_{ds} \neq 0$, i.e. latent heat is extracted from the surface. This lowers the surface temperature, which enhances the downward sensible heat flux, which in turn extracts heat from the lower atmosphere, cooling the near-surface air [*Lenaerts et al.*, 2010]. These two effects, moistening and cooling of the surface layer which subsequently propagate into the full atmospheric boundary layer, through the model turbulent mixing scheme, are the main impacts of drifting snow on the atmosphere.

[28] In RACMO, the vertical diffusion of heat and moisture in the surface layer (SL, between surface and the first model layer at ~7–8 m above the surface) is calculated in a similar fashion to vertical diffusion in the atmospheric boundary layer (ABL) above the SL. The main difference is in the lower boundary condition, which in the SL is represented by the surface, i.e. the no-slip condition for momentum, the surface energy balance for heat and saturation with respect to ice for moisture. In (rare) very strong drifting snow events , drifting snow sublimation can occur up to tens or hundreds of meters above the surface [*Mahesh et al.*, 2003], i.e., well above the RACMO SL. For these strong events, prescribing the thermodynamic effects of drifting snow to occur in the SL means that the response in the ABL is delayed, with a timescale governed by the intensity of the vertical diffusion. However, under such strong wind conditions, this vertical mixing is vigorous, effectively limiting the delay. Quantifying this delay would require (1) accurate drifting snow concentration to be available at all lower model layers and (2) including a prognostic equation for the conservation of drifting snow particles in the RACMO ABL scheme. Such an effort is currently not warranted, because of the lack of evaluation data (no detailed measurements of vertical drifting snow profiles up to these heights exist to date).

[29] In addition, the model does not explicitly consider the effect of drifting snow particles on the absorption of solar radiation in the air, but as drifting snow in Antarctica is most active in winter, this effect is believed to be of minor importance.

[30] The erosion of snow by drifting snow (ER_{ds}) is defined as the divergence of the horizontal transport of suspended snow ($\nabla \cdot \mathbf{TR}_{ds}$). To determine ER_{ds} at each grid point, the horizontal transport vectors are needed, not only locally, but also from neighboring grid points. The horizontal transport scalar from the drifting snow routine is decomposed in two horizontal vector components using the wind vector at the lowest model level, assuming that wind and snow transport have the same direction. Finally, both SU_{ds} and ER_{ds} exchange mass with the surface. Therefore, both processes are introduced as mass fluxes in the snow model of RACMO2.1/ANT.

2.4. Fresh Snow Density as a Measure for $u_{*,t}$

[31] Due to the large spatial variability in wind speed, accumulation and temperature, surface snow characteristics vary greatly over the Antarctic continent [*Van den Broeke*, 2008]. Elsewhere, fresh snow may have a low density (typically 50–100 kg m^{-3}), but in the windy environment of Antarctica, snow crystal breaking and rounding rapidly densifies the snow at the surface [*Li and Pomeroy*, 1997; *Gallée et al.*, 2001]. As a result, surface snow density typically varies between 300–350 kg m^{-3}. An important negative feedback is the following: when erosion and/or sublimation remove the low-density top layer of the snowpack, compacted snow layers with a higher density are exposed. That, in turn, reduces the likelihood of additional drifting snow (drifting snow-density feedback).

[32] Measurements of surface snow density in Antarctica are sparse in time and space, and usually performed along overland traverses [e.g., *Richardson et al.*, 1997; *Anschütz et al.*, 2009] or as point measurements [*Van den Broeke*, 2008]. Near-surface snow density has been parameterized as a function of annual average surface temperature (T_s), 10 m wind speed (U_{10m}) and annual accumulation (Acc) [*Kaspers et al.*, 2004]. However, this frequently included density values are representative for the first 0.5–1 m of snow, while we are interested in the skin layer density (first few cm) for the purpose of drifting snow applications.

[33] *Loewe* [1970] analyzed drifting snow frequency data for 18 Antarctic stations (Figure 1), mainly collected during the IGY (1957–1958). For each station, he calculated a drifting snow frequency histogram for various wind speeds. Here we present a new formulation for the density of fresh Antarctic snow, which mainly determines the density of the surface snow, such that modeled drifting snow frequency fits these observations.

[34] We apply an iterative procedure to obtain a fresh snow density that best fits the observed drifting snow frequency for each station. For this purpose, we use the RACMO2.1/ANT data (DRIFT simulation), using the same numerical setup as discussed above. First, a quality check on the RACMO2.1/ANT wind data is performed (see Table 2). Stations 4 and 10 have been removed because of insufficient representation of the local katabatic wind regime, which results in an underestimation of the observed wind speed. Due to its sheltered positions, Wilkes (station 15) is characterized by weak katabatic winds, which are overestimated by RACMO2.1/ANT. This station is therefore also removed. Charcot (station 3) is removed because the drifting snow frequency was reported to be 100% for all wind speeds, which is clearly unrealistic. The other 14 stations show reasonable wind speed statistics in RACMO2.1/ANT.

[35] As a second step, the 10 m wind speed frequency distribution is calculated for the location of each of the 14 remaining stations. Because of lacking wind speed spectra from the observations from Loewe, we use the spectra from six-hourly RACMO2.1/ANT data (1989–2006) instead. To remove the remaining model bias, we correct the wind speeds in RACMO with the difference between the mean observed wind speed and the modeled wind speed (0–2.4 m s^{-1}). The measured [*Loewe*, 1970] drifting snow frequency spectrum is fitted to a Weibull distribution, from which we obtain an exact drifting snow frequency for each wind speed. The total drifting snow frequency (SDFR, Table 2) is then obtained by summing all drifting snow frequencies over the complete wind speed spectrum. Drifting snow frequency varies greatly among the stations (Table 2), with values ranging from 7% on the high Antarctic Plateau to 81% in windy (katabatic) regions.

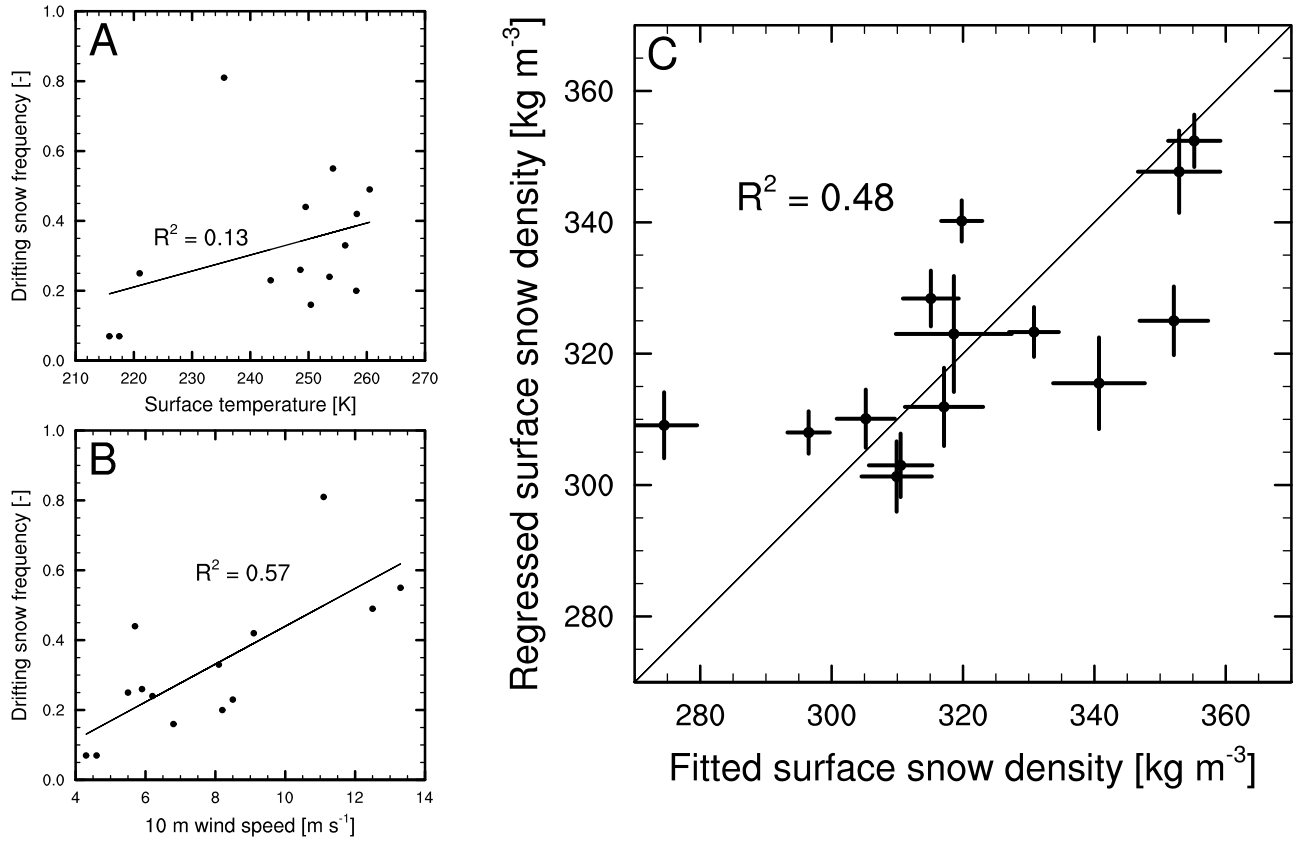

Figure 3. The regression of fresh snow density upon surface temperature (Figure 3a) and 10 m wind speed (Figure 3b) during accumulation for the period 1989–2006. The scatter between the density retrieved from the fitting procedure (horizontal) and the resulting fresh snow density from the regression (vertical) is shown in Figure 3c. The error bars show twice the standard deviation retrieved from 18 years of data. The error in the regressed density is assumed to be equal to the error in the fitting procedure. The squared correlation coefficient (R^2) is shown for Figures 3a, 3b, and 3c, together with the linear regression line in Figures 3a and 3b.

[36] Next, a starting value of ρ_s is assumed, providing $u_{*,t}$ (using DE = SP = 0.5). The six-hourly data from RACMO2.1/ANT (1989–2006) are again used to calculate drifting snow frequency as the fraction of time steps for which u_* exceeds $u_{*,t}$. While varying ρ_s, we repeat this procedure until modeled and observed drifting snow frequency agree within 2%. This exercise was repeated for each of the 18 years in the simulation to capture the interannual variability of fresh snow density, that could subsequently be used as a measure for the uncertainty in the fitting procedure (Figure 3), considering the fact that we only have 1–2 years of SDFR observations.

[37] The results of this exercise are summarized in Table 2. Values for ρ_{fit} (the fitted fresh snow density) vary between 275 and 355 kg m^{-3}. ρ_{fit} is low for stations in the interior, where wind speed, accumulation and surface temperature are low. Eights, which has a relatively high accumulation rate, but a low wind speed, also has a low fresh snow density. High ρ_{fit} values are found at stations with relatively high wind speed, accumulation and temperature (S2 and Mirny), but also at e.g. Byrd station. This is because at this site, SDFR is relatively low (23%) in combination with a mean wind speed of 8.5 m s^{-1}. As a result, the fresh snow density obtained here is high. This also holds for Halley Bay.

[38] Finally, the fresh snow density thus obtained is regressed upon other known model parameters, to be able to calculate fresh snow density in the model during accumulation events. Table 2 and Figures 3a and 3b suggest that ρ_{fit} is related to annual mean surface temperature (as a measure for rate of snow metamorphosis) and/or 10 m wind speed during accumulation (as a measure for the wind-induced breaking and rounding of snow particles). Pionerskaya is an outlier. Here, drifting snow frequency is very high (81%), but the mean 10 m wind speed during accumulation is not extremely high (11 m s^{-1}) and the mean surface temperature is only 235 K. Probably, local surface conditions facilitate drifting snow; the station is located in the escarpment zone where the topography has a convex form (Figure 1), which is usually associated with convergence of snow by the wind. This continuously renews the top snow layer and keeps its density low, which favors drifting snow.

[39] The multiple linear regression that relates fresh snow density to mean surface temperature ($T_{sfc,Acc}$) and 10 m wind speed ($U_{10m,Acc}$) during accumulation, becomes

$$\rho_{reg} = A + BT_{sfc,Acc} + CU_{10m,Acc} \quad (11)$$

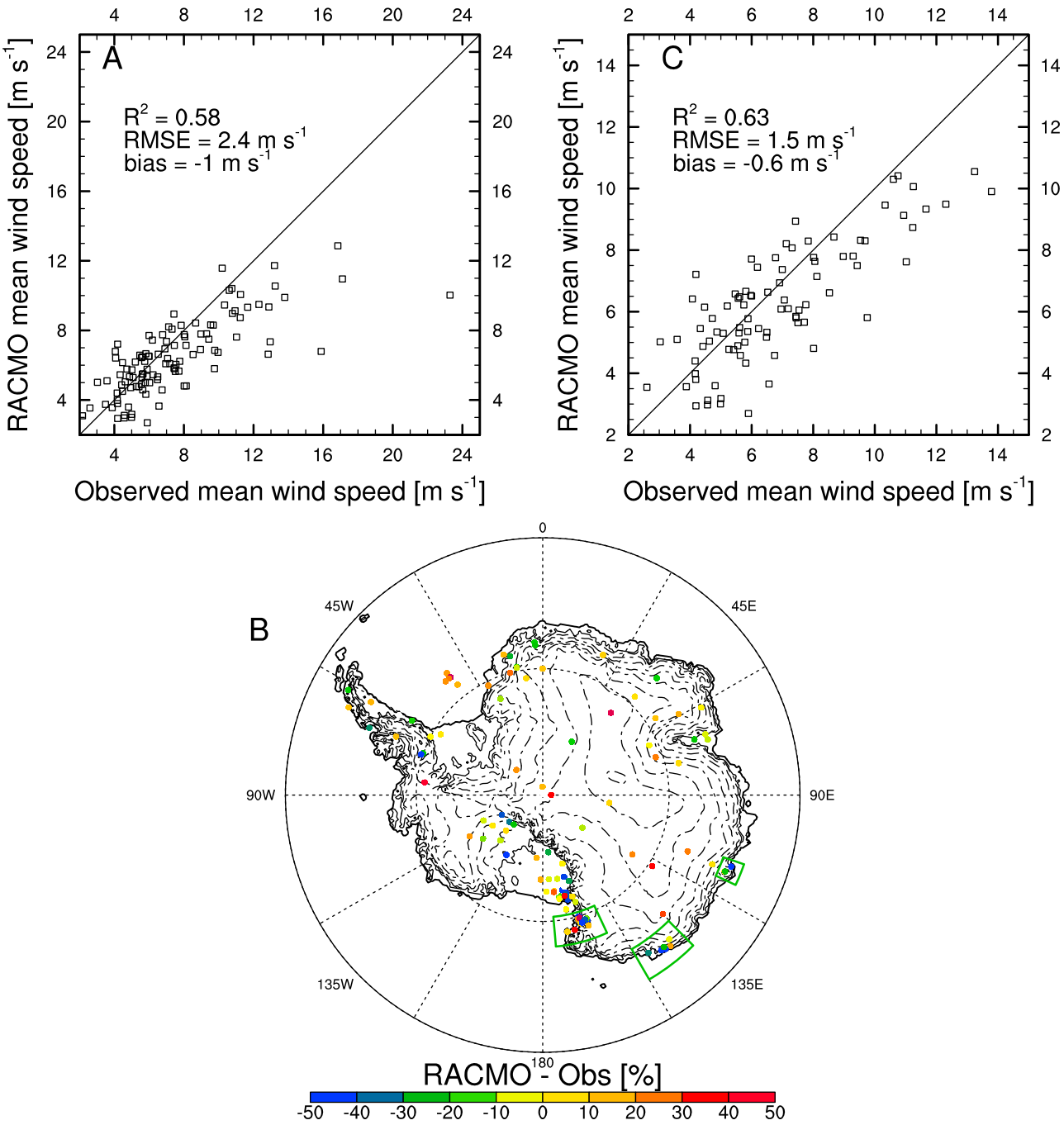

Figure 4. Wind speed (10 m height) validation of RACMO2.1/ANT at 115 stations in Antarctica. (a) Modeled versus observed mean wind speed (mean of monthly values for the overlapping period). (b) Performance of RACMO2.1/ANT depending on location; shown is the deviation from RACMO with respect to the observations (%), so a negative/positive value is associated with an under/overestimation by the model. (c) Same as Figure 4a but without the 23 stations located within the green rectangles in Figure 4b.

where A = 97.5 kg m^{-3}, B = 0.77 kg m^{-3} K^{-1} and C = 4.49 kg s m^{-4}.

[40] Including annual total accumulation in the regression procedure did not improve the fit. Figure 3 shows that all regressed values are within 30 kg m^{-3} of the fitted values, corresponding to an uncertainty in $u_{*,t}$ of ~0.1 m s^{-1}. In general, stations with high wind speed and/or temperature are characterized by a higher fresh snow density. We used this relation in RACMO2.1/ANT to compute fresh snow density during each accumulation event. By doing so, the values of ρ_s and the conditions for drifting snow are strongly linked to the local 'accumulation' climate. As an additional condition, the minimum/maximum fresh snow density is set to 300/350 kg m^{-3}, which are reasonable limits for ρ_s [*Kaspers et al.*, 2004].

Table 1. Overview and Source of Station Data Used in the Wind Speed Validation of RACMO2.1/ANT

Alias	Name	Number of Stations
USAP	Antarctic Meteorological Research Center, University of Wisconsin-Madison	78
AUST	Australian Antarctic Division Glaciology Program	16
ITA	Italian Antarctic Research Programme	10
IMAU	Institute for Marine and Atmospheric Research, Utrecht University	9
IPF	International Polar Foundation (Princess Elizabeth Base)	1
BAS	British Antarctic Survey (Halley station)	1

[41] To summarize, the effect of surface snow densification through high wind during snowfall as well as the surfacing of high density snow in erosion areas is explicitly included in RACMO2.1/ANT; the model does not explicitly simulate the formation of wind crusts, because their formation mechanism and how they impact drifting snow is still poorly understood.

3. Model Evaluation

[42] Two RACMO2.1/ANT simulations were performed. The first simulation (DRIFT) includes the drifting snow physics and the interactions with the atmosphere and snow surface, as described in this section. In the second simulation (NODRIFT) drifting snow is de-activated. We performed two years of model integration (1989–1990) to initialize the snowpack, and used the snowpack structure of 1 January 1991 as initial condition for the full model simulation (January 1989–December 2009).

3.1. Near-Surface Climate

[43] To correctly model drifting snow, the near-surface wind speed field needs to be realistically simulated. We find that the differences between DRIFT and NODRIFT are small [*Lenaerts and van den Broeke*, 2012], and not significant compared to the differences between model and observations. Therefore we show results from the DRIFT simulation only. Figure 4 compares the mean monthly wind speed for overlapping periods between observations and model for 115 automatic weather stations (AWS) in Antarctica. The station data are compiled from various sources (Table 1) and have a good coverage over the Antarctic ice sheet (Figure 4b). Before analysis, a thorough quality test was performed on the data [*Sanz Rodrigo*, 2011]. Stations with less than 1 year of data are removed. Data with spurious gaps or irregular behavior are omitted as well.

[44] Given that all data come from AWS, with known problems for quality control, the correlation between modeled and observed wind speed is high, especially for wind speeds below 10 m s^{-1}. Stations with very high wind speeds are not well represented in RACMO2.1/ANT, which explains the relatively low correlation coefficient in Figure 4a. Figure 4b suggests that the largest underestimation occurs in regions with complex topography, such as the Transantarctic Mountains, around Cape Denison, where very high annual mean wind speeds occur (>20 m s^{-1}), and around Law Dome. When the stations located in these areas are removed (Figure 4c), the agreement considerably improves. The squared correlation coefficient (R^2) increases from 0.48 to 0.64 and the root-mean squared error (RMSE) and mean bias decrease substantially. As drifting snow is closely related to wind speed, we should realize that potentially very strong drifting snow events in these regions may

Table 2. Drifting Snow and Near-Surface Climate Characteristics of the Drifting Snow Stations [*Loewe*, 1970] Used for the Fresh Snow Density Fitting and Regression Procedure[a]

Number	Name	SDFR	$U_{10m,M}$ (m s^{-1})	$U_{10m,O}$ (m s^{-1})	Acc (mm)	T_s (K)	ρ_{fit} (kg m^{-3})	ρ_{reg} (kg m^{-3})	$u_{*,t}$ (m s^{-1})
1	Byrd	0.23	7.7	8.4	120	243.5	352.1	325.0	0.46
2	Pionerskaya	0.81	10.0	11.1	151	235.5	319.8	340.2	0.35
5	South Pole	0.25	5.5	5.5	56	221.0	296.5	308.0	0.28
6	Sovietskaya	0.07	5.4	4.3	31	217.5	309.9	301.3	0.32
7	Plateau	0.07	5.1	4.6	18	215.8	310.5	303.0	0.32
8	Eights	0.44	5.4	5.6	537	249.5	274.5	309.1	0.22
9	Maudheim	0.33	8.3	7.6	335	256.3	318.6	323.0	0.35
11	Baudoin	0.42	7.5	7.9	351	258.3	315.1	328.4	0.34
12	Ellsworth	0.24	7.0	6.0	294	253.6	317.1	311.9	0.34
13	Halley Bay	0.16	7.0	6.9	529	250.4	340.7	315.5	0.42
14	Syowa	0.20	5.7	7.6	173	258.2	330.8	323.3	0.39
16	S2	0.49	9.4	11.7	665	260.5	352.9	347.7	0.46
17	Mirny	0.55	10.1	12.5	881	254.2	355.2	352.4	0.47
18	Little America	0.26	6.0	5.9	201	248.6	305.2	310.1	0.31
3	Charcot	1	9.6	9.0					
4	South Ice	…	6.4	11.5					
10	Mawson	…	7.6	11.8					
15	Wilkes	…	7.5	5.8					

[a]Listed are station number (see Figure 1) and name, observed total drifting snow frequency (SFDR), mean 10 m wind speed in RACMO2.1/ANT (1989–2006, $U_{10m,M}$) and in the observations (1957–1958, $U_{10m,O}$), mean annual accumulation (RACMO 2.1/ANT, 1989–2006, Acc), mean surface temperature (RACMO 2.1/ANT, 1989–2006, T_s), fitted (ρ_{fit}) and regressed (ρ_{reg}) fresh snow density, and resulting mean threshold friction velocity ($u_{*,t}$). The bottom four rows are stations that have been excluded.

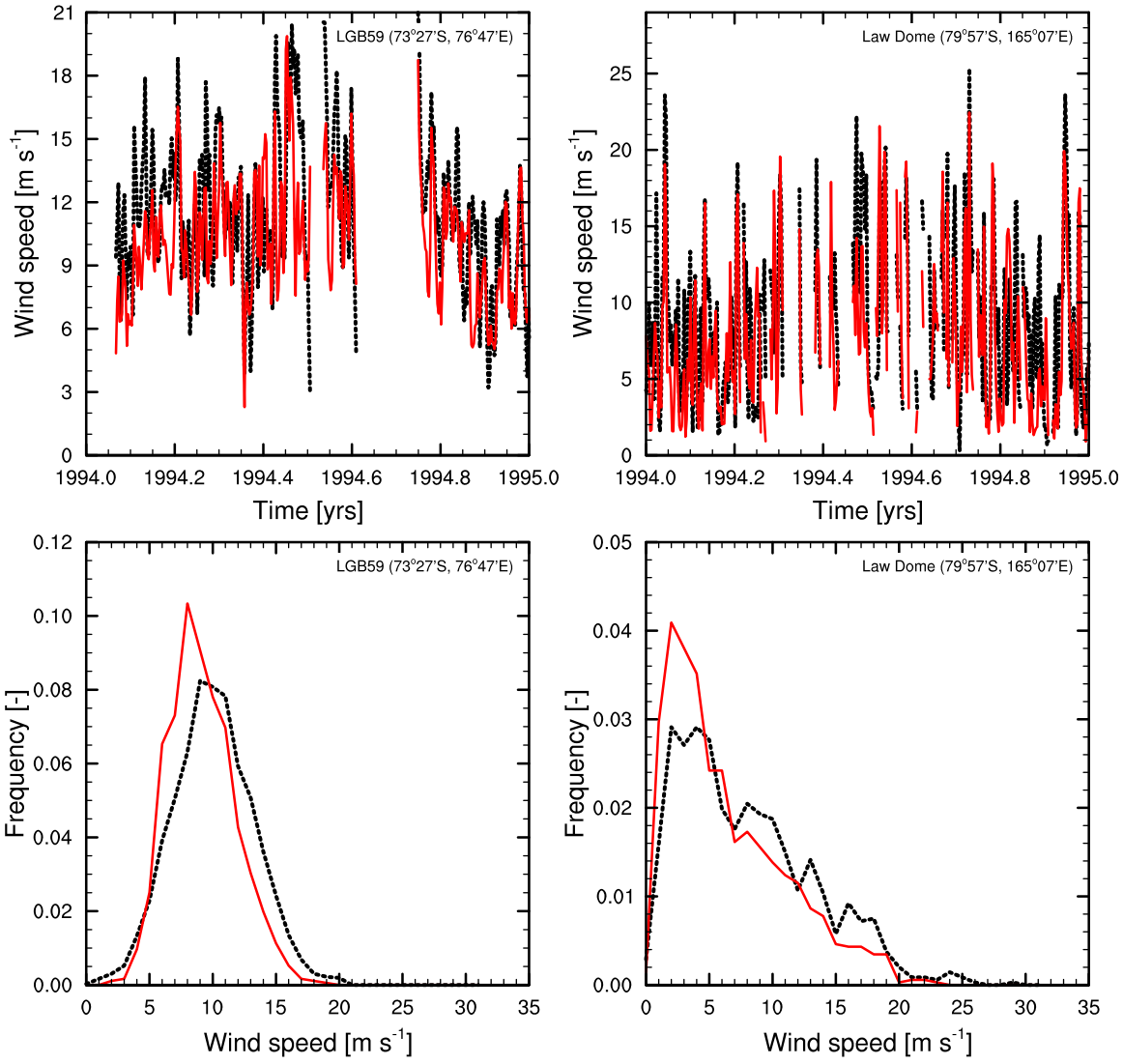

Figure 5. Observed (black) and modeled (red) 10 m daily mean wind speed time series of available data in 1 year (1994, top) and distribution (bottom) at two stations in Antarctica for the overlapping periods, i.e., 1994–2003 for LGB59 and 1989–1998 for Law Dome. Note the different scales.

not be modeled correctly. On the other hand, we are aware that the locations of some of these stations are not representative for their surroundings, so we expect some of these high wind speeds to be local.

[45] In Antarctica, two main wind regimes are found; first, the ice sheet escarpment is characterized by katabatic winds flowing from the interior toward the coast. Secondly, coastal stations have a wind climate that is strongly influenced by low-pressure systems, i.e. near-surface winds are mainly 'synoptically driven'. Figure 5 shows wind time series for one year and frequency distributions (based on daily data) for those two wind regimes. The AWS LGB59 is located in the Lambert Glacier basin, at an elevation of 2300 m above sea level. The wind speed is normally distributed, with a mean wind speed and maximum frequency around 10 m s^{-1}. This wind climate can be characterized as 'katabatic-dominated', with limited variability in wind speed and direction. At Law Dome, located near the coast, katabatic forcing is absent and storm passages are frequent. The highest wind frequency is around 4 m s^{-1}, but the distribution is strongly skewed and tails off slowly with relatively frequent occurrences of high wind speeds and associated drifting snow events. The wind speed variability and distribution at both locations is well reproduced by RACMO2.1/ANT.

[46] Near-surface temperature to a large extent determines moisture content and sublimation potential. It must therefore be correctly simulated. Although the surface energy balance is different in drifting snow conditions, the near-surface temperature in DRIFT is not significantly changed compared to NODRIFT. Therefore, it is not possible to assess whether including drifting snow leads to better representation of near-surface temperature. Figure 6 shows the seasonal cycle (based on monthly means) of observed and modeled 2 m temperature at 5 Antarctic stations. The overall correspondence is good, but the winters in RACMO2.1/ANT at the coastal stations (4 and 5) are too cold. A possible reason is

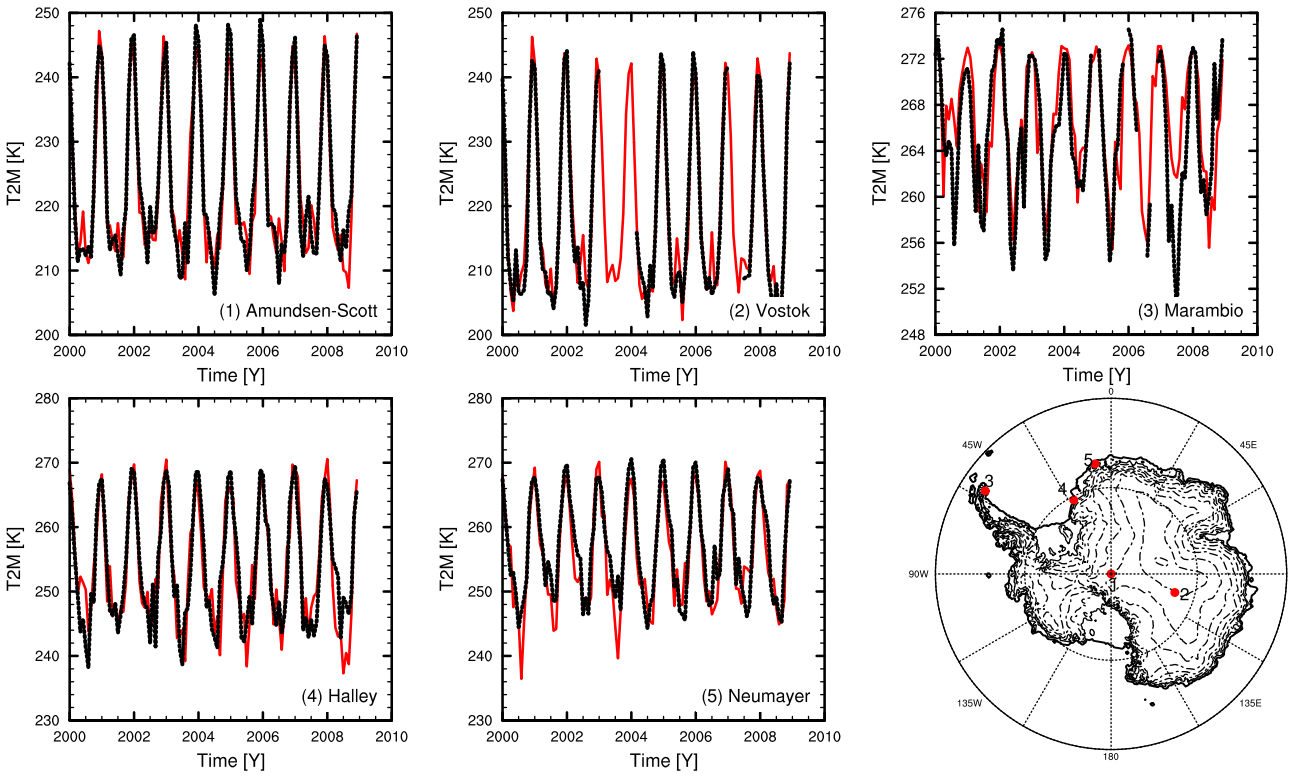

Figure 6. Observed (black; source, SCAR READER database (http://www.antarctica.ac.uk/met/READER/)) and modeled (red) monthly mean 2 m temperatures (K). The locations of the stations are shown on the map. The modeled values of stations 3, 4, and 5 are located on the first inland (100% land) point to avoid errors related to land-sea interactions.

the underestimation of incoming longwave radiation from the atmosphere [*Van de Berg et al.*, 2007; *Ettema et al.*, 2010b], which is probably related to an underestimation of atmospheric moisture in winter and/or an underestimation of the clear-sky radiance [*Van de Berg et al.*, 2007]. Figure 7 shows that RACMO2.1/ANT captures the wide range of annual mean surface temperatures (mainly obtained from 10 m deep snow temperature). The underestimation at the warmer coastal stations follows the wintertime bias discussed above.

[47] Apart from near-surface wind speed and temperature, SU_{ds} also strongly depends on near-surface relative humidity, as this determines the potential for sublimation in the lower atmosphere [*Lenaerts et al.*, 2010]. Due to SU_{ds}, 2 m relative humidity (with respect to ice), is clearly higher in DRIFT compared to NODRIFT (Figure 8a). The difference is most pronounced in the coastal regions of East Antarctica, where drifting snow is strong. There we locally find an increase of RH_i of 10% or more. At Neumayer base, this moisture increase leads to a more realistic seasonal cycle of near-surface relative humidity (Figure 8b), although RH_i remains slightly underestimated. At this station, located on an ice shelf in coastal Dronning Maud Land (71°S, 8°E), drifting snow sublimation removes around 16% of the annual precipitation [*Lenaerts et al.*, 2010]. The observed annual mean RH_i is 91% for the period 1993–2007, whereas the DRIFT simulation gives 87% and the NODRIFT simulation 85% for the same period. The RH_i increase from summer to winter is much better represented in the DRIFT simulation. This indicates that the higher moisture content due to enhanced SU_{ds} in winter, together with lower temperatures in winter, explains the strong seasonal cycle of near-surface RH_i at Neumayer.

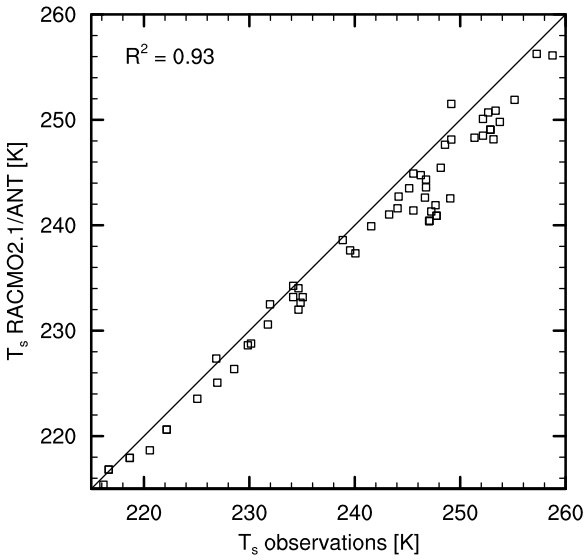

Figure 7. Mean modeled (1989–2009) and observed (obtained from 10 m deep snow temperature [*Van den Broeke*, 2008]) mean surface temperature (K) for 64 locations in Antarctica.

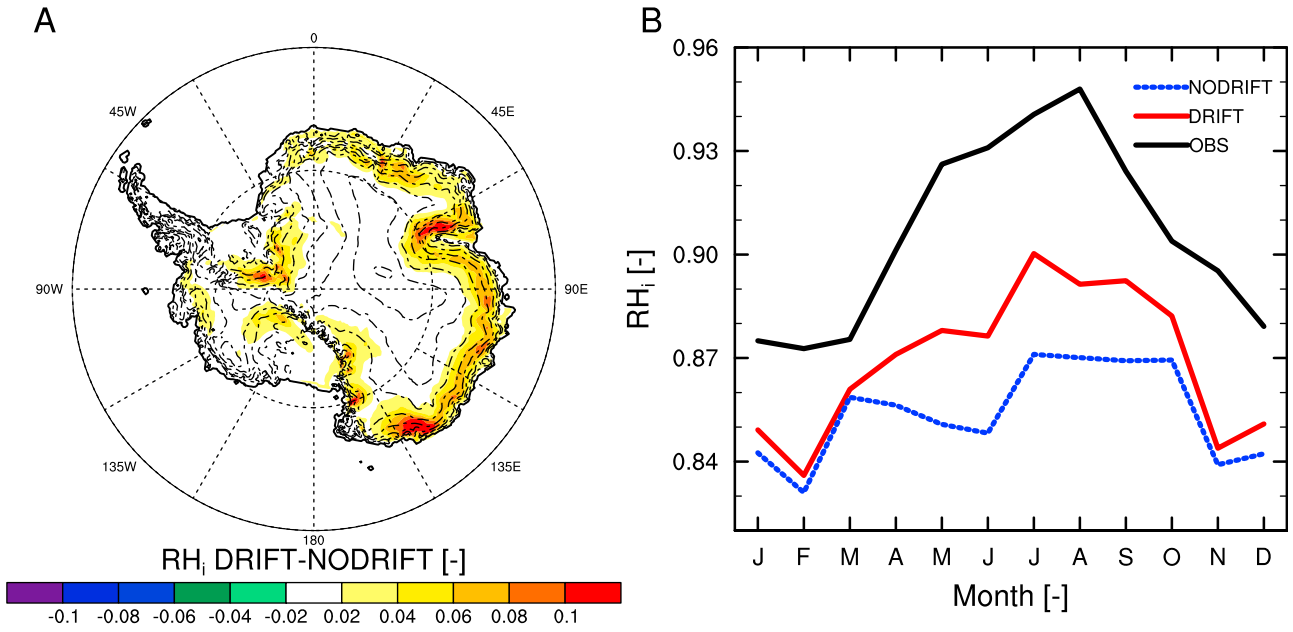

Figure 8. (a) Difference between the mean (1989–2009) 2 m relative humidity (with respect to ice) in DRIFT and NODRIFT. (b) Annual cycle of 2 m relative humidity (with respect to ice) at Neumayer station, according to the observations (black), DRIFT (red), and NODRIFT (blue) for the period 1993–2007.

3.2. Drifting Snow Frequency

[48] With respect to the drifting snow process, drifting snow frequency is the best observable parameter that can still serve to evaluate model drifting snow results. Problems could arise from the assumption that surface snow density equals fresh snow density, as densification could enhance surface density between the time of snowfall and the first drifting snow event, especially in the calm interior ice sheet. Figure 9 shows that this is not prohibitive for the method. RACMO2.1/ANT is able to realistically simulate the frequency of drifting snow at these stations. The most important underestimation is seen at Eights, which has a clearly higher fresh snow density than expected from the observed drifting snow distribution (see Table 2). At Pionerskaya, the station with the largest drifting snow frequency, SDFR is somewhat underestimated. This can be explained by the fact that RACMO2.1/ANT underestimates the highest wind speeds (Figure 4). The high overall correlation indicates that the new parameterization of surface snow density leads to a realistic representation of drifting snow frequencies over a wide range of climate conditions, and supports our empirical approach.

[49] A first independent check is performed by comparing observed and modeled drifting snow frequency at Neumayer station, East Antarctica, a station which is not included in the procedure to determine ρ_s. Figure 10 illustrates the temporal variability of drifting snow frequency observed at Neumayer and modeled by RACMO2.1/ANT. The interannual variability is significant (Figure 10a), with measured annual mean drifting snow frequency ranging from 27% to 36%. This variability is very well reproduced by the model. Drifting snow frequency also varies strongly within the year, from ~20% in summer, increasing to ~40% in mid-winter. Despite a small overestimation, RACMO2.1 captures this intra-annual variability well (Figure 10b). In summer there is a very subtle feedback at play: in the drifting snow run, enhanced sublimation exposes older snow layers with larger grains. This lowers the surface albedo and enhances melt. This in turn prohibits drifting snow, because melt further densifies the surface snow and makes it even darker. At locations where snowmelting is marginal, such as Neumayer, an overestimation of this melt triggers this feedback and may already lead to densification that is too strong, prohibiting drifting snow, while in reality drifting snow still

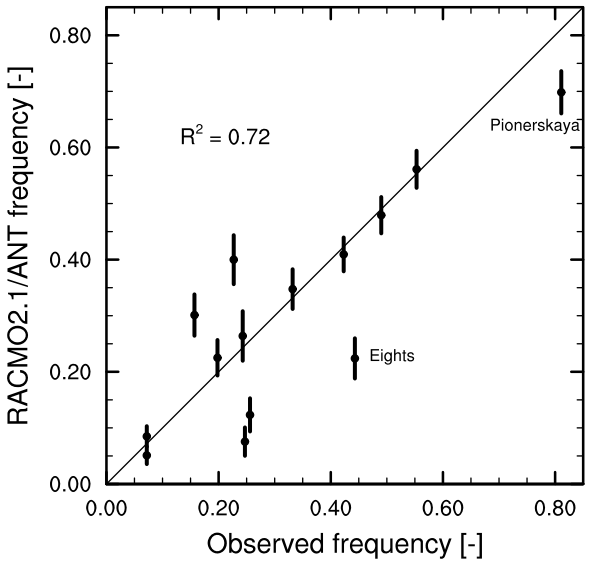

Figure 9. Modeled (1989–2009) and observed (1957–1958) drifting snow frequency for the stations in Table 2. The lengths of the vertical bars denote twice the standard deviation of annual values based on the period 1989–2009.

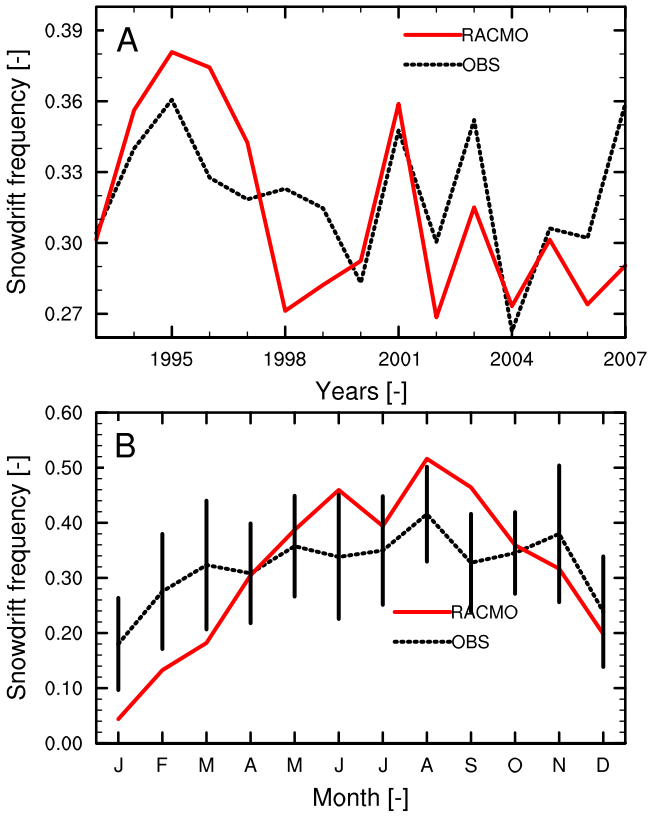

Figure 10. (a) Interannual and (b) seasonal variability of drifting snow frequency at Neumayer from observations (black) and the model (red) for the period 1993–2007. The vertical black bars denote twice the standard deviation of the observations.

occurs. But melting can also be discontinuous is space, so that another plausible explanation is that the observed drifting snow is advected from upwind areas where melting did not take place. Finally, there is the uncertainty in the observations to take into account. In winter, RACMO2.1/ANT slightly overestimates drifting snow frequency. This wintertime result is satisfactory given the fact that all variables on which drifting snow frequency depends are generated internally in RACMO: wind speed, accumulation amount and frequency, temperature and wind speed during accumulation and melt events, the latter which are very infrequent at Neumayer. On top of that, there is the uncertainty in the observation, which could be biased by changes in observer and/or observation time.

[50] Although uncertainties are significant, some studies reported estimates of horizontal transport of snow in Antarctica using optical or impact sensors [*Bintanja et al.*, 2001; *Nishimura and Nemoto*, 2005; *Frezzotti et al.*, 2007]. From a region that is well-known for its strong katabatic winds, *Scarchilli et al.* [2010] reported a mean drifting snow frequency of 80% and a cumulative snow transport of $5 \cdot 10^6$ kg m^{-1} in the period 2006–2007 at Larsen Glacier in Victoria Land (74°57′S, 161°46′E, 1350 m a.s.l.). The modeled total transport in RACMO2.1/ANT ($4.6 \cdot 10^6$ kg m^{-1}) in the same period for this location agrees very well with these observations. The modeled drifting snow frequency is 60% for 2006 and 65% for 2007, which is somewhat lower than the measurements by *Scarchilli et al.* [2010]. At Halley station, located on an ice shelf in coastal Antarctica (75°35′S, 26°34′W), the cumulative snow transport in austral winter of 1991 was estimated to be $5.5 \cdot 10^5$ kg m^{-1} [*Mann et al.*, 2000]. Our model somewhat overestimates the snow transport ($7.3 \cdot 10^5$ kg m^{-1}), but the modeled snow frequency (29%) is well within the observed range (27–37% [*Mann et al.*, 2000]).

[51] These local drifting snow measurements are essential for model evaluation, but they are sparse and not always representative for large areas. In that respect, remote sensing offers promising new tools to provide drifting snow characteristics over extended areas. Here, we use a novel product, namely drifting snow frequencies derived from IceSAT and/or CALIPSO satellites. The algorithm, which is described in detail by *Palm et al.* [2011], uses the satellite backscatter signal to detect thick (>20 m) drifting snow layers. Although the application of this technique is limited to cloud-free regions where the drifting snow is strong enough, it provides insight in the spatial and temporal variability of drifting snow over almost the entire Antarctic ice sheet [*Palm et al.*, 2011]. The technique is applied to a full year (2009) of CALIPSO tracks (almost 35 million single point measurements). Next, Antarctica is split up in 1 × 1 degree grid cells, in which the drifting snow frequency is defined as the ratio between the number of drifting snow events and the total number of cloud-free events. To facilitate a direct comparison, we used 3-hourly RACMO2.1/ANT data, removed all data with cloud cover higher than 5% and snow transport lower than 0.15 kg m^{-1} s^{-1}, which is equivalent to a drifting snow layer depth of ∼20 m. Figure 11 shows the comparison between the CALIPSO-derived drifting snow frequency and modeled drifting snow frequency from RACMO2.1/ANT for July 2009. We choose this month because it has the highest drifting snow frequency of the whole year 2009. The spatial patterns in RACMO generally match very well with CALIPSO. The model agrees with CALIPSO on the high drifting snow frequencies in Victoria and Adélie Land [*Palm et al.*, 2011]. Modeled drifting snow frequencies are higher in coastal areas of East Antarctica, whereas the band of high frequencies is somewhat more confined to the coast. Although the uncertainties involved with this comparison are significant, this result provides evidence that the spatial distribution of drifting snow is realistically modeled in RACMO2.1/ANT.

3.3. Surface Ablation

[52] Figure 12 identifies ablation areas (SMB < 0) in the DRIFT simulation. While there is only one clear ablation area in the NODRIFT simulation (around the Lambert Glacier, not shown), in the DRIFT simulation the combined effect of drifting snow sublimation and erosion (Figure 12a) causes ablation areas to appear along the Transantarctic Mountains (Figure 12b), in Dronning Maud Land and around the Lambert Glacier basin (Figure 12c). All of these areas are known as meteorite collection sites (Figure 12), providing qualitative support for the modeled distribution of ablation areas. Several other meteorite collection sites

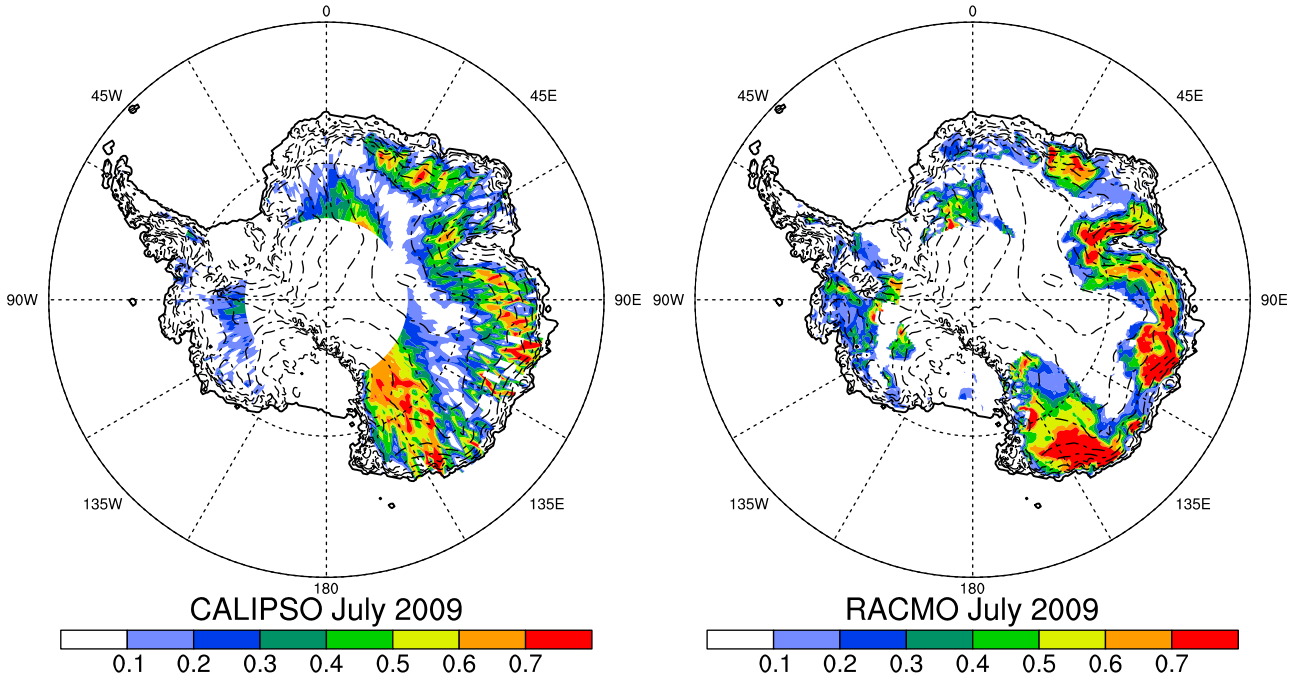

Figure 11. Drifting snow frequency in July 2009 (left) derived from CALIPSO [*Palm et al.*, 2011] and (right) modeled by RACMO2.1/ANT. Note that these plots only show strong drifting snow events in noncloudy conditions (see section 3.2).

coincide with areas with low (<50 mm yr^{-1}) modeled SMB values. Including drifting snow in the model increases the spatial extent of ablation areas in Antarctica from 0.1 to 0.5%, much closer to the satellite-retrieved extent of 0.8% given by *Winther et al.* [2001]. These findings indicate that the drifting snow process is essential to retrieve a realistic location and extent of ablation areas in Antarctica.

4. Summary and Conclusions

[53] For the first time, an interactive routine that calculates drifting snow transport and sublimation has been coupled to a three-dimensional regional climate model and subsequently run to simulate drifting snow in Antarctica for a period long enough to generate a useful climatology (1989–2009).

[54] First we evaluated the near-surface Antarctic climate in RACMO2.1/ANT. Due to its relatively fine horizontal resolution (~27 km), RACMO2.1/ANT captures most local climate conditions; only in topographically complex environments with strong winds, a significant wind speed underestimation is found. In these topographically rough areas, AWS wind speed observations are not always representative for a larger area, as cold katabatic flows are strongly influenced by the topography, which is not adequately resolved by the current model resolution of 27 km. Modeled near-surface and surface temperatures agree well with observations, apart from a negative winter bias, mainly as coastal stations, caused by an underestimation of incoming longwave radiation. Drifting snow has no significant impact on the temperature and wind speed near the surface, but increases relative humidity, which becomes more realistic compared to observations.

[55] Next, we used observed drifting snow frequencies, obtained during the IGY (1957–1958), to develop an empirical parameterization for fresh snow density, using local temperature and wind speed as predictors. In combination with a density-dependent formulation of threshold friction velocity, this approach generates realistic drifting snow frequencies around the continent.

[56] Evaluation of modeled drifting snow characteristics is difficult owing to the near-complete absence of observations of drifting snow from Antarctica. In spite of the relative simplicity of the drifting snow routine, and the fact that all climate parameters that are important for drifting snow (surface snow density, snowfall, temperature, wind speed) are internally generated by RACMO2.1/ANT and hard to verify due to a lack of observations, good qualitative agreement is found with drifting snow frequency observations and total transport estimates at three Antarctic locations: Halley, Neumayer and Victoria Land. An improved continent-wide distribution of ablation areas is found when drifting snow is activated, and RACMO2.1/ANT is capable of qualitatively reproducing the frequency of heavy drifting snow events detected by laser altimetry from space [*Palm et al.*, 2011]. A more detailed analysis of the differences, which remain substantial at places, must wait until more reliable drifting snow observations from Antarctica become available.

[57] These results enable a quantitative analysis of the drifting snow climate in Antarctica, as presented in part 2 of this paper.

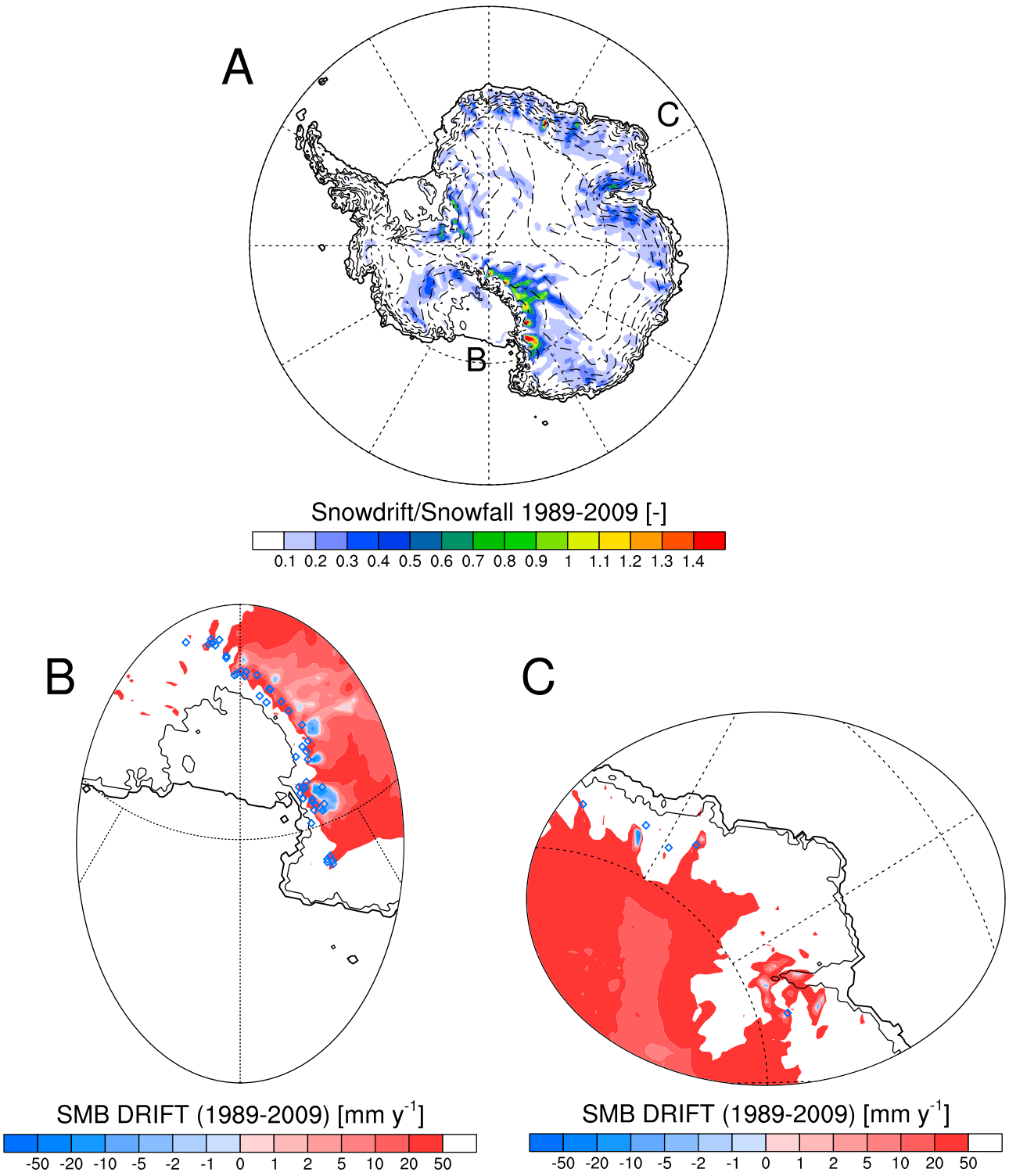

Figure 12. (a) Mean (1989–2009) ratio of drifting snow (SU_{ds} + ER_{ds}) to snowfall. (b and c) Annual mean SMB in DRIFT (1989–2009), the color scale focusing on SMB values marginally different from zero, with negative SMB values in blue and positive values in red. Figure 12b shows Ross ice shelf and Transantarctic Mountains. Figure 12c shows Lambert Basin, Eastern Dronning Maud Land, and Enderby Land. SMB values above 50 mm yr^{-1} are not shown. In Figures 12b and 12c, the locations of meteorite deposition sites are represented by open blue diamonds.

[58] **Acknowledgments.** We thank two anonymous reviewers for their valuable comments. This work was supported by funding from the ice2sea program from the European Union 7th Framework Programme, grant 226375. This is Ice2sea contribution number 059.

References

Anschütz, H., K. Müller, E. Isaksson, J. R. McConnell, H. Fischer, H. Miller, M. Albert, and J. G. Winther (2009), Revisiting sites of the South Pole Queen Maud Land Traverses in East Antarctica: Accumulation data from shallow firn cores, *J. Geophys. Res.*, *114*, D24106, doi:10.1029/2009JD012204.

Arthern, R. J., D. G. Vaughan, A. M. Rankin, R. Mulvaney, and E. R. Thomas (2010), In situ measurements of Antarctic snow compaction compared with predictions of models, *J. Geophys. Res.*, *115*, F03011, doi:10.1029/2009JF001306.

Bintanja, R. (1998), The interaction between drifting snow and atmospheric turbulence, *Ann. Glaciol.*, *26*, 167–173.

Bintanja, R. (2000), Snowdrift suspension and atmospheric turbulence: Part 2. Results of model simulations, *Boundary Layer Meteorol.*, *95*, 369–395.

Bintanja, R. (2001), Modelling snowdrift sublimation and its effect on the moisture budget of the atmospheric boundary layer, *Tellus, Ser. A*, *53*, 215–232.

Bintanja, R., and C. H. Reijmer (2001), A simple parameterization for snowdrift sublimation over Antarctic snow surfaces, *J. Geophys. Res.*, *106*(D23), 31,739–31,748.

Bintanja, R., and M. R. van den Broeke (1995), The surface energy balance of Antarctic snow and blue ice, *J. Appl. Meteorol.*, *34*, 902–926.

Bintanja, R., H. Lilienthal, and H. Tüg (2001), Observations of snowdrift over Antarctic snow and blue ice surfaces, *Ann. Glaciol.*, *32*, 168–174.

Box, J. E., D. H. Bromwich, B. A. Veenhuis, L. S. Bai, J. C. Stroeve, J. C. Rogers, K. Steffen, T. Haran, and S. H. Wang (2006), Greenland ice sheet surface mass balance variability (1988–2004) from calibrated polar MM5 output, *J. Clim.*, *19*(12), 2783–2800.

Bromwich, D. H., Z. Guo, L. Bai, and Q. Shen (2004), Modeled Antarctic precipitation: part i. Spatial and temporal variability, *J. Clim.*, *17*(3), 427–447, doi:10.1175/1520-0442(2004)017.

Budd, W. F. (1966), The drifting of nonuniform snow particles, in *Studies in Antarctic Meteorology*, *Antarct. Res. Ser.*, vol. 9, edited by M. J. Rubin, pp. 59–70, AGU, Washington, D. C.

Déry, S. J., and M. K. Yau (1999), A bulk blowing snow model, *Boundary Layer Meteorol.*, *93*(2), 237–251.

Déry, S. J., and M. K. Yau (2001), Simulation of blowing snow in the Canadian Arctic using a double-moment model, *Boundary Layer Meteorol.*, *99*(2), 297–316.

Ettema, J., M. R. van den Broeke, E. van Meijgaard, W. J. van de Berg, J. L. Bamber, J. E. Box, and R. C. Bales (2009), Higher surface mass balance of the Greenland ice sheet revealed by high-resolution climate modeling, *Geophys. Res. Lett.*, *36*, L12501, doi:10.1029/2009GL038110.

Ettema, J., M. R. van den Broeke, E. van Meijgaard, and W. J. van de Berg (2010a), Climate of the Greenland ice sheet using a high-resolution climate model: Part 1. Evaluation. *Cryosphere*, *4*(2), 511–527, doi:10.5194/tc-4-511-2010.

Ettema, J. E., M. R. van den Broeke, E. van Meijgaard, W. J. van de Berg, J. E. Box, and K. Steffen (2010b), Climate of the Greenland ice sheet using a high-resolution climate model: Part 2. Near-surface climate and energy balance, *Cryosphere*, *4*, 529–544, doi:10.5194/tc-4-529-2010.

Fettweis, X. (2007), Reconstruction of the 1979–2006 Greenland ice sheet surface mass balance using the regional climate model MAR, *Cryosphere*, *1*, 21–40, doi:10.5194/tc-1-21-2007.

Frezzotti, M., et al. (2005), Spatial and temporal variability of snow accumulation in East Antarctica from traverse data, *J. Glaciol.*, *51*, 113–124.

Frezzotti, M., S. Urbini, M. Proposito, C. Scarchilli, and S. Gandolfi (2007), Spatial and temporal variability of surface mass balance near Talos Dome, East Antarctica, *J. Geophys. Res.*, *112*, F02032, doi:10.1029/2006JF000638.

Fujii, Y., and K. Kusunoki (1982), The role of sublimation and condensation in the formation of ice sheet surface at Mizuho Station, Antarctica, *J. Geophys. Res.*, *87*, 4293–4300.

Gallée, H., G. Guyomarch, and E. Brun (2001), Impact of snow drift on the Antarctic ice sheet surface mass balance: Possible sensitivity to snow-surface properties, *Boundary Layer Meteorol.*, *99*, 1–19.

Garratt, J. R. (1992), *The Atmospheric Boundary Layer*, Cambridge Univ. Press, New York.

Genthon, C., and G. Krinner (2001), Antarctic surface mass balance and systematic biases in general circulation models, *J. Geophys. Res.*, *106*, 20,653–20,664.

Hyland, R. W., and A. Wexler (1984), Formulations for the thermodynamic properties of the saturated phases of H_2O from 173.15 K to 473.15 K, *ASHRAE Trans.*, *89*, 500–519.

Jackson, B. S., and J. J. Carroll (1978), Aerodynamic roughness as a function of wind direction over asymmetric surface elements, *Boundary Layer Meteorol.*, *14*(3), 323–330, doi:10.1007/BF00121042.

Kaspers, K. A., R. S. W. van de Wal, M. R. van den Broeke, J. Schwander, N. P. M. van Lipzig, and C. A. M. Brenninkmeijer (2004), Model calculations of the age of firn air across the Antarctic continent, *Atmos. Chem. Phys.*, *4*, 1365–1380.

King, J. C., and P. S. Anderson (1994), Heat and water vapour fluxes and scalar roughness lengths over an Antarctic ice shelf, *Boundary Layer Meteorol.*, *69*(1–2), 101–121.

Kuipers Munneke, P., M. R. van den Broeke, J. T. M. Lenaerts, M. G. Flanner, A. S. Gardner, and W. J. van de Berg (2011), A new albedo scheme for use in climate models over the Antarctic ice sheet, *J. Geophys. Res.*, *116*, D05114, doi:10.1029/2010JD015113.

Lenaerts, J. T. M., and M. R. van den Broeke (2012), Modeling drifting snow in Antarctica with a regional climate model: 2. Results, *J. Geophys. Res.*, *117*, D05109, doi:10.1029/2010JD015419.

Lenaerts, J. T. M., M. R. van den Broeke, S. J. Déry, G. König-Langlo, J. Ettema, and P. Kuipers Munneke (2010), Modelling snowdrift sublimation on an Antarctic ice shelf, *The Cryosphere*, *4*(2), 179–190, doi:10.5194/tc-4-179-2010.

Lenaerts, J. T. M., M. R. van den Broeke, W. J. van de Berg, E. van Meijgaard, and P. Kuipers Munneke (2012), Present-day (1989–2009) high-resolution surface mass balance of Antarctica from a regional atmospheric climate model, *Geophys. Res. Lett.*, doi:10.1029/2011GL050713, in press.

Lettau, H. (1969), Note on aerodynamic roughness-parameter estimation on the basis of roughness-element description, *J. Appl. Meteorol.*, *8*(5), 828–832.

Li, L., and J. W. Pomeroy (1997), Estimates of threshold wind speeds for snow transport using meteorological data, *J. Appl. Meteorol.*, *36*(3), 205–213.

Liljequist, G. H. (1956), *Energy Exchange of an Antarctic Snow-Field*, 298 pp., Norsk Polarinst., Oslo.

Loewe, F. (1970), The transport of snow on ice sheets by the wind, in *Studies on Drifting Snow*, edited by U. Radok, pp. 21–69, Dep. of Meteorol., Univ. of Melbourne, Parkville, Vict., Australia.

Mahesh, A., R. Eager, J. R. Campbell, and J. D. Sphinhirne (2003), Observations of blowing snow at the South Pole, *J. Geophys. Res.*, *108*(D22), 4707, doi:10.1029/2002JD003327.

Mann, G. W., P. S. Anderson, and S. D. Mobbs (2000), Profile measurements of blowing snow at Halley, Antarctica, *J. Geophys. Res.*, *105* (D19), 24,491–24,508.

Nishimura, K., and M. Nemoto (2005), Blowing snow at Mizuho station, Antarctica, *Philos. Trans. R. Soc. A*, *363*, 1647–1662.

Palm, S. P., Y. Yang, J. Spinhirne, and A. Marshak (2011), Satellite remote sensing of blowing snow properties over Antarctica, *J. Geophys. Res.*, *116*, D16123, doi:10.1029/2011JD015828.

Pimienta, P., and P. Duval (1987), Rate controlling processes in the creep of polar glacier ice, *J. Phys. Colloques*, *48*, C1-243–C1-248, doi:10.1051/jphyscol:1987134.

Pomeroy, J. W., and R. L. H. Essery (1999), Turbulent fluxes during blowing snow: Field tests of model sublimation predictions, *Hydrol. Processes*, *13*(18), 2963–2975.

Reijmer, C. H., E. van Meijgaard, and M. R. van den Broeke (2004), Numerical studies with a regional atmospheric climate model based on changes in the roughness length for momentum and heat over Antarctica, *Boundary Layer Meteorol.*, *111*(2), 313–337.

Reijmer, C. H., E. van Meijgaard, and M. R. van den Broeke (2005), Evaluation of temperature and wind over Antarctica in a Regional Atmospheric Climate Model using 1 year of Automatic Weather Station data and upper air observations, *J. Geophys. Res.*, *110*, D04103, doi:10.1029/2004JD005234.

Richardson, C., E. Aarholt, S.-E. Hamran, P. Holmlund, and E. Isaksson (1997), Spatial distribution of snow in western Dronning Maud Land, East Antarctica, mapped by a ground-based snow radar, *J. Geophys. Res.*, *102*(B9), 20,343–20,353.

Rignot, E., J. L. Bamber, M. R. van den Broeke, C. Davis, Y. Li, W. J. van de Berg, and E. van Meijgaard (2008), Recent Antarctic ice mass loss from radar interferometry and regional climate modelling, *Nat. Geosci.*, *1*(2), 106–110.

Sanz Rodrigo, J. (2011), On Antarctic wind engineering, Ph.D. thesis, Univ. Libre de Bruxelles, Brussels. [Available at http://theses.ulb.ac.be/ETD-db/collection/available/ULBetd-03152011-235458.]

Scarchilli, C., M. Frezzotti, P. Grigioni, L. De Silvestri, L. Agnoletto, and S. Dolci (2010), Extraordinary blowing snow transport events in east Antarctica, *Clim. Dyn.*, *34*, 1195–1206, doi:10.1007/s00382-009-0601-0.

Simmons, A., S. Uppala, D. Dee, and S. Kobayashi (2007), Era-interim: New ECMWF reanalysis products from 1989 onwards, *ECMWF Newsl.*, *110*, 29–35.

Turner, J., W. M. Connelley, S. Leonard, G. J. Marshall, and D. G. Vaughan (1999), Spatial and temporal variability of net snow accumulation over the Antarctic from ECMWF re-analysis project data, *Int. J. Climatol.*, *19*(7), 697–724.

Undén, P., et al. (2002), HIRLAM-5 scientific documentation, technical report, Swed. Meteorol. and Hydrol. Inst., Norrköping, Sweden.

Van As, D., M. R. van den Broeke, and M. M. Helsen (2007), Strong-wind events and their impact on the near-surface climate at Kohnen station on the Antarctic plateau, *Antarct. Sci.*, *19*(4), 507–519.

Van de Berg, W. J., M. R. van den Broeke, C. H. Reijmer, and E. van Meijgaard (2005), Characteristics of the Antarctic surface mass balance (1958–2002) using a regional atmospheric climate model, *Ann. Glaciol.*, *41*, 97–104.

Van de Berg, W. J., M. R. van den Broeke, C. H. Reijmer, and E. van Meijgaard (2006), Reassessment of the Antarctic surface mass balance using calibrated output of a regional atmospheric climate model, *J. Geophys. Res.*, *111*, D11104, doi:10.1029/2005JD006495.

Van de Berg, W. J., M. R. van den Broeke, and E. van Meijgaard (2007), Heat budget of the East Antarctic lower atmosphere derived from a regional atmospheric climate model, *J. Geophys. Res.*, *112*, D23101, doi:10.1029/2007JD008613.

Van den Broeke, M. R. (2008), Depth and density of the Antarctic firn layer, *Arct. Antarct. Alp. Res.*, *40*(2), 432–438.

Van den Broeke, M. R., J. G. Winther, E. Isaksson, J. F. Pinglot, L. Karlöf, T. Eiken, and L. Conrads (1999), Climate variables along a traverse line in Dronning Maud Land, East Antarctica, *J. Glaciol.*, *45*(150), 295–302.

Van den Broeke, M. R., W. J. van de Berg, E. van Meijgaard, and C. H. Reijmer (2006), Identification of Antarctic ablation areas using a regional atmospheric climate model, *J. Geophys. Res.*, *111*, D18110, doi:10.1029/2006JD007127.

Van den Broeke, M. R., G. C. König-Langlo, G. Picard, P. Kuipers Munneke, and J. T. M. Lenaerts (2010), Surface energy balance, melt and sublimation at Neumayer Station, East Antarctica, *Antarct. Sci.*, *22*(1), 87–96.

Van Meijgaard, E., L. H. van Ulft, W. J. van de Berg, F. C. Bosvelt, B. J. J. M. Van den Hurk, G. Lenderink, and A. P. Siebesma (2008), The KNMI regional atmospheric model RACMO version 2.1, *Tech. Rep., 302*, R. Neth. Meteorol. Inst. (KNMI), De Bilt, Netherlands.

Velicogna, I. (2009), Increasing rates of ice mass loss from the Greenland and Antarctic ice sheets revealed by GRACE, *Geophys. Res. Lett.*, *36*, L19503, doi:10.1029/2009GL040222.

Weller, G. (1980), Spatial and temporal variations in the south polar surface energy balance, *Mon. Weather Rev.*, *108*, 2006–2014.

Wendler, G., N. Ishikawa, and Y. Kodama (1988), The heat balance of the icy slope of Adelie Land, Eastern Antarctica, *J. Appl. Meteorol.*, *27*(1), 52–65.

White, P. W. (2001), Physical processes (CY23R4), technical report, Eur. Cent. for Med. Range Weather Forecasts, Reading, U. K.

Winther, J. G., M. N. Jespersen, and G. E. Liston (2001), Blue-ice areas in Antarctica derived from NOAA avhrr satellite data, *J. Glaciol.*, *47*(157), 325–334.

Xiao, J. B., R. Bintanja, S. J. Dery, G. W. Mann, and P. A. Taylor (2000), An intercomparison among four models of blowing snow, *Boundary Layer Meteorol.*, *97*(1), 109–135.

Yang, J., and M. Yau (2008), A new triple-moment blowing snow model, *Boundary Layer Meteorol.*, *126*(1), 137–155, doi:10.1007/s10546-007-9215-4.

S. J. Déry, Northern Hydrometeorology Group, University of Northern British Columbia, Prince George, BC 000 000, Canada.

J. T. M. Lenaerts, W. J. van de Berg, and M. R. van den Broeke, Institute for Marine and Atmospheric Research Utrecht, Utrecht University, Princetonplein 5, Utrecht NL-3584 CC, Netherlands. (jtmlenaerts@gmail.com)

S. P. Palm, Science Systems and Applications, Inc., NASA Goddard Space Flight Center, Code 613.1, Greenbelt, MD 20771, USA.

J. Sanz Rodrigo, Von Karman Institute for Fluid Dynamics, Chaussé de Waterloo, B-1640 Rhode-St.-Genese, Belgium.

E. van Meijgaard, Royal Netherlands Meteorological Institute, PO Box 201, De Bilt NL-3730 AE, Netherlands.